

Stripes in thin ferromagnetic films with out-of-plane anisotropy

D. Clarke, O. A. Tretiakov, and O. Tchernyshyov
*Johns Hopkins University, Department of Physics and Astronomy,
 3400 N. Charles St., Baltimore, Maryland 21218*

We examine the $T = 0$ phase diagram of a thin ferromagnetic film with a strong out-of-plane anisotropy (e.g. Co/Pt multilayers) in the vicinity of the reorientation phase transition. The phase diagram in the anisotropy-applied field plane is universal in the limit in which the film thickness is the shortest length scale. It contains uniform fully magnetized and canted phases, as well as periodically nonuniform states: weakly modulated spin-density waves and strongly modulated stripes. We determine the boundaries of metastability of these phases and point out the existence of a critical point at which the difference between the SDW and striped phases vanishes. Out-of-plane magnetization curves exhibit hysteresis loops caused by the coexistence of one or more phases. Additionally, we study the effect of a system edge on the orientation of nearby stripes. We compare our results with recent experiments.

I. INTRODUCTION

Recent experimental studies have revealed rich physics of thin ferromagnetic films with an easy axis of magnetization normal to the film plane.^{1,2,3,4,5,6,7,8} Such films possess several magnetic phases in which the magnetization can be uniformly normal to the plane, canted, or periodically modulated in one direction (striped). Magnetization curves exhibit intricate magnetic hysteresis indicating coexistence of phases. Magnetic probes with sub-micron resolution provide detailed information about nucleation and growth of new domains during the magnetization reversal.¹ These developments fuel the need for a theoretical understanding of ferromagnetism in thin films.

Theoretical studies of thin films with magnetic moments pointing out of the plane date back to the 1980s.⁹ The simplest model describes Ising spins with local ferromagnetic exchange and long-range dipolar interactions. A competition between these forces makes the uniform ferromagnetic states unstable towards a spontaneous formation of magnetic stripes with an alternating sign of the magnetization. The stripe period is a mesoscopic length determined by the relative strengths of exchange and dipolar interactions.

A major drawback of the dipolar Ising model is the neglect of the in-plane components of magnetization, which become important when the magnetization rotates away from the plane normal, a process known as the reorientation phase transition (RPT). A minimal model must therefore use a three-dimensional vector of magnetization whose magnitude M is considered fixed well below the Curie temperature and whose orientation is given by the colatitude θ and azimuth ϕ : $\mathbf{M} = M(\sin\theta\cos\phi, \sin\theta\sin\phi, \cos\theta)$ with the z axis normal to the film plane xy . In a state with uniform magnetization, the energy density contains the easy-axis anisotropy $-K\cos^2\theta$ and the demagnetizing term $(\mu_0/2)M^2\cos^2\theta$ due to the magnetic field. In the absence of an applied field the RPT occurs when the anisotropy drops below the critical strength $K_0 = \mu_0 M^2/2$.

The assumption of uniform magnetization breaks down in the vicinity of the RPT: as in the dipolar Ising model, the competition between local and long-range forces leads to the formation of stripes with a mesoscopic period that depends on the effective anisotropy $K - K_0$, exchange strength A , and the film thickness t .¹⁰ Depending on the anisotropy and on the strength of an applied magnetic field, the stripes can appear as a weak spin-density wave (SDW) in the background of uniform magnetization or as fairly wide domains of uniform magnetization separated by narrow domain walls.

The presence of the in-plane components of magnetization leads to an important distinction of domain walls from their counterparts in the Ising model: the vector of magnetization *rotates* between the (mostly) upward and downward directions. Thus domain walls are endowed with in-plane magnetization, a fact with important topological consequences. The domain walls are of the Bloch type: the in-plane magnetization on them points along the wall. In contrast to Neel walls (in-plane magnetization normal to the wall), Bloch walls do not generate stray magnetic field and thus have a lower magnetic energy. We will therefore specialize to magnetization configurations in which the vector of magnetization depends on a single coordinate x and lies in the yz plane:

$$\mathbf{M} = M(0, \sin\theta(x), \cos\theta(x)). \quad (1)$$

Using a variational approach, Berger and Erickson¹¹ obtained a phase diagram of such a one-dimensional model as a function of the anisotropy $K - K_0$ and an applied out-of-plane field H_\perp . It exhibits several phases with both first and second-order transitions between them. Berger and Erickson focussed on *thermodynamic* transitions and did not provide boundaries of metastability. Such boundaries are important for the understanding of magnetic hysteresis in thin films. Often thermal activation is insufficient to initiate the decay of a metastable phase and magnetization reversal begins only when that phase becomes locally unstable.

In this work we describe several new results. Our main achievement is the determination of out-of-plane magnetization curves $M_\perp(H_\perp)$ that can be directly compared

with experimental data. We show that, for sufficiently thin films, the shape of the magnetization curve depends on a single parameter that is a function of the dimensionless effective anisotropy $\kappa = (K - K_0)/K_0$, film thickness t , and the magnetic exchange length $\lambda = \sqrt{2A/\mu_0 M^2}$. This universality is the consequence of a scaling property of the free energy in the thin-film limit. A proper rescaling of the anisotropy κ and magnetic field H_\perp yields a universal phase diagram. We point out the existence of critical points of the liquid-gas type that terminate lines of thermodynamic first-order phase transitions between striped and SDW phases. Finally, we discuss the behavior of stripes near the edge of the film. We find a tendency for stripes to meet an edge perpendicularly, independent of the particular shape of stripe.

The formalism used in this work is minimization of the free energy. The average out-of-plane magnetization in a sample with stripes is chiefly dependent on the average period of those stripes rather than their orientational or translational order. We thus neglect the influence of thermal fluctuations, which tend to disrupt that orientational and translational order in the stripe phase.^{12,13}

The paper is organized as follows. In Section II we derive the functional of magnetic free energy specialized to one-dimensional variations, describe its scaling properties in a thin-film limit, and introduce appropriately rescaled variables. We illustrate its use by finding the lines of instability of the uniform phases in the anisotropy-applied field phase diagram. In Section III we determine the boundaries of metastability of nonuniform phases and magnetization curves using a numerical minimization. We also find the location of the stripe-SDW critical points in the (K, H_\perp) plane. Section IV deals with the behavior of stripes near the film edge. Some useful intermediate results are described in the Appendixes.

II. THE MODEL

A. The free energy

The free-energy functional for a thin ferromagnetic film of thickness t can be separated into a local and long-range parts. The local part includes the exchange, uniaxial anisotropy, and Zeeman energies:

$$E_{\text{local}} = t \int d^2r \left(A |\nabla \hat{\mathbf{m}}|^2 - K m_z^2 - \mu_0 M \mathbf{H} \cdot \hat{\mathbf{m}} \right), \quad (2)$$

where $\hat{\mathbf{m}} = (\sin \theta \cos \phi, \sin \theta \sin \phi, \cos \theta)$ is the three-dimensional unit vector pointing along the magnetization and $\nabla = (\partial_x, \partial_y)$ is the two-dimensional gradient in the plane of the film. The long-range part is due to dipolar interactions:

$$E_{\text{dipolar}} = \frac{\mu_0 M^2}{4\pi} \int d^2r \int d^2r' m_z(\mathbf{r}) V(\mathbf{r} - \mathbf{r}') m_z(\mathbf{r}'), \quad (3)$$

where the dipolar kernel $V(\mathbf{r}) = 1/r - 1/\sqrt{r^2 + t^2}$ reflects the interaction of magnetic charges with densities $\pm M m_z(\mathbf{r})$ induced on the top and bottom surfaces of the film. The expression for the dipolar energy (3) is valid provided that there are no magnetic charges in the bulk of the film, i.e. $\partial_x m_x + \partial_y m_y = 0$. This condition is compatible with Eq. (1), which describes a system with Bloch domain walls. Domain walls of the Neel type generate additional dipolar terms.

Specializing to one-dimensional configurations without bulk magnetic charges (1), and with magnetic field applied perpendicular to the plane of the film, we obtain the energy

$$\begin{aligned} \frac{E}{L_y t} = & \int dx \left[A (d\theta/dx)^2 - K \cos^2 \theta - \mu_0 M H \cos \theta \right] \\ & + \frac{1}{2} \mu_0 M^2 \int dx \int dx' \cos \theta(x) V(x - x') \cos \theta(x'), \end{aligned} \quad (4)$$

where L_y is the width of the system in the y direction. The one-dimensional kernel $V(x) = (1/2\pi t) \ln(1 + t^2/x^2)$ obtained by integrating (3) over y has the Fourier transform

$$\tilde{V}(k) = \frac{1 - e^{-|k|t}}{|k|t} = 1 - \frac{|k|t}{2} + \mathcal{O}(t^2). \quad (5)$$

The Taylor expansion (5) is justified when the film thickness t is the shortest length scale in the problem. The zeroth-order term $\tilde{V}_0(k) = 1$ can be interpreted as a contact part of the dipolar interaction that simply shifts the anisotropy: $K \mapsto K - K_0$. The first-order term $\tilde{V}_1(k) = -|k|t/2$ represents the effect of the stray dipolar field. Its inverse Fourier transform $V_1(x)$ diverges at short length scales and requires a short-range cutoff. It has the following properties:

$$V_1(x) \sim \frac{t}{2\pi x^2} \text{ as } x \rightarrow \infty, \quad \int dx V_1(x) = 0. \quad (6)$$

B. Scaling property of the free energy

It is convenient to use natural scales for various physical units: $K_0 = \mu_0 M^2/2$ for the effective anisotropy κ and volume energy density, and M for magnetic field:

$$\kappa = (K - K_0)/K_0, \quad \mathbf{h} = \mathbf{H}/M. \quad (7)$$

In these units,

$$\frac{E_{\text{local}}}{\mu_0 M^2 L_y t} = \int dx \left[\frac{\lambda^2}{2} \left(\frac{d\theta}{dx} \right)^2 - \frac{\kappa}{2} \cos^2 \theta - h \cos \theta \right] \quad (8)$$

and

$$\frac{E_{\text{stray}}}{\mu_0 M^2 L_y t} = \frac{1}{2} \int dx \int dx' \cos \theta(x) V_1(x - x') \cos \theta(x'), \quad (9)$$

where $\lambda = \sqrt{A/K_0}$ is the exchange length.

The free energy, given by the sum of these terms, is invariant under a scaling transformation

$$x \mapsto bx, \quad t \mapsto t, \quad \lambda \mapsto b^{1/2}\lambda, \quad \kappa \mapsto b^{-1}\kappa, \quad \mathbf{h} \mapsto b^{-1}\mathbf{h}. \quad (10)$$

This symmetry indicates that the state of the film depends on the effective anisotropy and magnetic field through scale-invariant variables κ/κ_0 and \mathbf{h}/κ_0 , where $\kappa_0 = t^2/(4\lambda)^2$ is an effective anisotropy scale whose significance will be clarified shortly. It also yields a characteristic length scale $8\pi\lambda^2/t$, which determines the period of the stripes—see Eq. (12) below.

The free energy is scale-invariant only to the lowest order in the film thickness t . Inclusion of higher-order terms in the dipolar kernel (5) violates this property. The scaling works as long as the thickness t is small compared to all other length scales, in particular the exchange length $\lambda \approx 5$ nm (for Co).

Note that this scaling law applies more generally to two-dimensional configurations with an applied field in any direction, as the energies associated with bulk magnetic charges and in plane fields are also invariant under (10) when t is small.

C. Uniform phases

Let us first discuss the uniform phases and their instabilities in the case that the applied field is normal to the plane. The case $\kappa > 0$ is trivial: only the upward and downward polarized states are stable. Both are locally stable in the region $|h| < \kappa$. The coexistence leads to a hysteresis in magnetization curves $m_z(h)$.

The situation is more interesting for $\kappa < 0$, where magnetization prefers the in-plane direction. In a uniform state the stray field vanishes and the energy is proportional to $-(\kappa/2)\cos^2\theta - h\cos\theta$. In a strong field, $|h| > |\kappa|$, the film is fully polarized, $\cos\theta = \text{sgn}(h)$. Below the critical strength, $|h| < |\kappa|$, the magnetization is canted, $\cos\theta = h/|\kappa|$. The uniform-to-canted transitions at $h = \pm\kappa$ are continuous.

Consider the free energy of small fluctuations around a canted state, $\cos\theta(x) = -h/\kappa + \delta(x)$:

$$\Delta E = \frac{\mu_0 M^2 L_y t}{2} \int \frac{dk}{2\pi} \left(\frac{\lambda^2 k^2}{\sin^2 \theta_0} - \kappa - \frac{|k|t}{2} \right) |\tilde{\delta}(k)|^2 + \mathcal{O}(\delta^4), \quad (11)$$

where $\tilde{\delta}(k)$ is the Fourier transform of $\delta(x)$ and $\cos\theta_0 = -h/\kappa$ is the equilibrium value for the canted state. The softest mode has the wavenumber

$$k_0 = \frac{t \sin^2 \theta_0}{4\lambda^2}. \quad (12)$$

A spin-density wave develops in the canted background on the line

$$(h/\kappa)^2 = 1 + \kappa/\kappa_0, \quad (13)$$

where $\kappa_0 = t^2/(4\lambda)^2$. An expansion to the order $\mathcal{O}(\delta^4)$ reveals a positive-definite quartic term. Thus the canted-SDW transition is also continuous. Note that the scaling arguments are confirmed: the wavelength is indeed set by the scale $8\pi\lambda^2/t$ and the critical line (13) contains the rescaled variables h/κ_0 and κ/κ_0 .

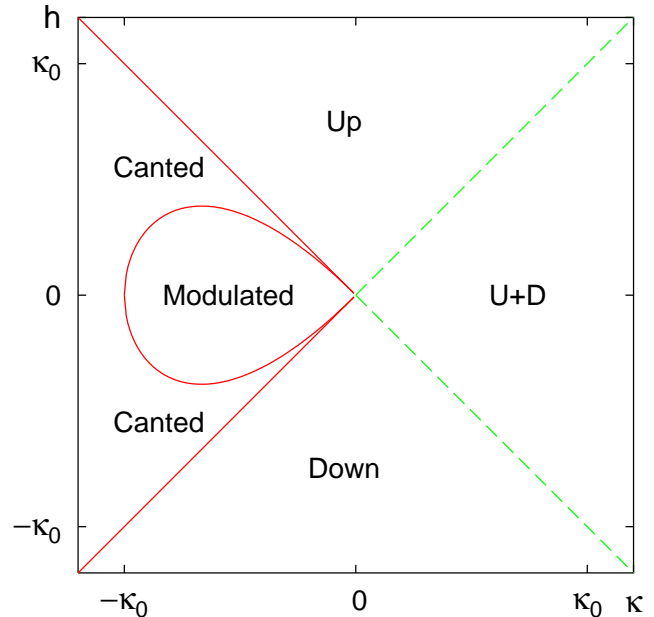


FIG. 1: (Color online) Phase diagram showing the regions of stability of uniform phases. Up (U) and Down (D) phases coexist in the region on the right. Solid and dashed lines denote continuous and discontinuous transitions, respectively.

Since no uniform solution is stable inside the semicubic parabola (13), this region must be occupied by an inhomogeneous state, which one might easily guess to be a stripe phase (see Fig. 1). However, the situation is somewhat more complicated. A further analysis shows that the stripe phase remains (at least locally) stable outside the semicubic curve. In addition, we find a region of coexistence between a strongly inhomogeneous striped state and a weakly inhomogeneous SDW state. Like a liquid and a gas, the two phases differ from each other only quantitatively. Indeed, there is a critical point at which the differences vanish continuously, as we will discuss below.

III. STRIPE PHASE

In this section, we describe the striped state in various regions of the h - κ plane. We determine the approximate boundaries of stability of the striped phase, and show how the metastability of the stripe phase leads to the hysteresis curves observed in experiments.

A. Numerical determination of metastability limits for the stripe phase

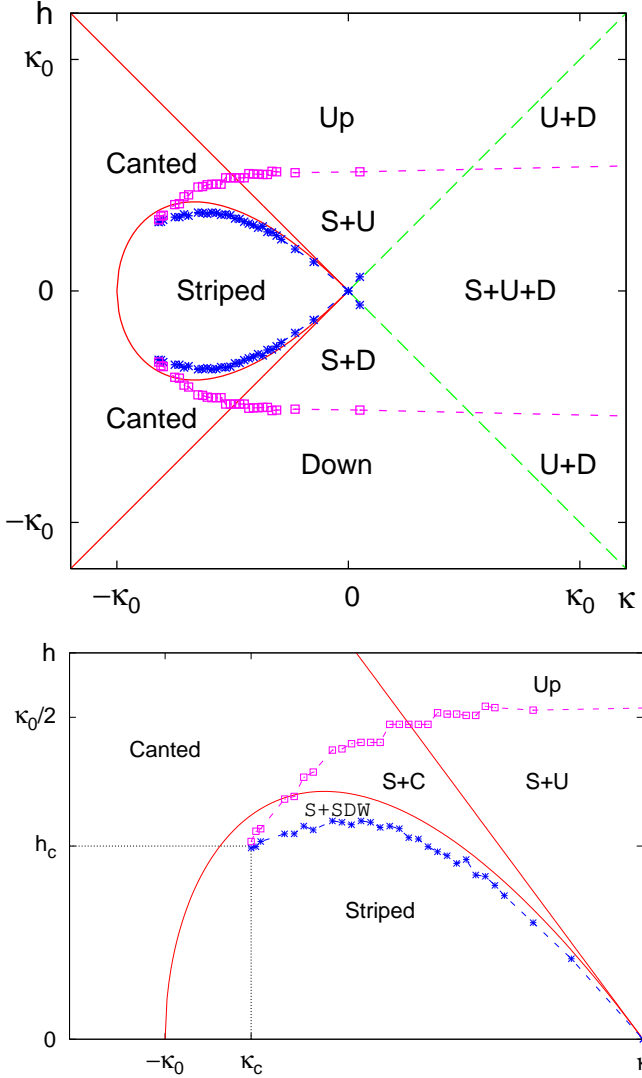


FIG. 2: (Color online) Numerically determined boundaries of the nonuniform phases are shown as symbols. The Striped phase can coexist with the Canted (C), Up (U), Down (D), and Spin density wave (SDW) states in various regions of the phase diagram. Solid and dashed lines denote continuous and discontinuous transitions, respectively.

In order to find the boundaries of stability of the striped phase, we performed a numerical simulation of the system described by Eqs. (8) and (9). The simulation was conducted on a chain of 2048 magnetization vectors of unit length described by the angle $\theta(x)$. Periodic boundary conditions were applied. We used specific values for the exchange length and thickness of 5 and 3 lattice spacings, respectively. However, based on the scaling arguments described in Section II B, we expect the results to be universal for thin films. Eq. (8) was mini-

mized using a relaxation method,¹⁴ where h was replaced by $h_{\text{eff}}(x) = h - \int dx' V_1(x - x') \cos \theta(x')$ to account for the dipolar stray field. This h_{eff} was recalculated after a number of iterations of the relaxation method. The process continued until the Lagrange equation,

$$\lambda^2(d^2\theta/dx^2) = \kappa \cos \theta \sin \theta + h_{\text{eff}} \sin \theta, \quad (14)$$

was satisfied at each point. Random noise was then added to the system and h was incremented. In this way, the algorithm moved the state of the system along the local minimum of energy. Sweeps of the magnetization were conducted from positive to negative values of h and the average magnetization was recorded. The hysteresis loops shown in Fig. 3 were produced from these single sweeps by rotating the data points to produce the upward sweep and superimposing it on the downward one. Discontinuous jumps in the magnetization mark the system's entry into and exit from the striped phase. In what follows, we interpret the resulting phase diagram (Fig. 2) for various values of the effective anisotropy.

An important feature of phase diagram revealed by the numerical simulation is the existence of liquid-gas like critical points at $\kappa_c \approx -0.82\kappa_0$, $h_c \approx \pm 0.3\kappa_0$ (Fig. 2). To the right of this point, a distinction can be made between a striped phase, with large modulation around a small average magnetization, and a spin-density wave phase, which has a small modulation around a larger average magnetization. Boundaries of metastability extend from the critical points, surrounding regions of coexistence between the striped and SDW phases. To the left of κ_c the two phases merge into one and magnetization curves proceed in a reversible manner. It is important to note that for $\kappa_c < \kappa < 0$, the second-order phase transition line out of the canted phase is very close to the first-order phase transition line into the striped phase. As such, this second-order transition may be difficult to detect as it is hidden by the nearby first-order jump.

In the remainder of this section, we describe the results of a sweep of the applied magnetic field beginning in high positive field normal to the sample and moving to a high negative field. The results of such a sweep depend on the anisotropy constant κ/κ_0 describing the system.

For strong enough in-plane anisotropy, $\kappa < -\kappa_0$, the striped phase is never seen. A sweep of magnetic field from high positive to high negative fields would find a completely reversible magnetization curve, with the uniform upward phase beginning to cant at $h = -\kappa$ and following the field smoothly and linearly. The magnetization will be $-h/\kappa$ until the field is decreased to the $h = \kappa$ line, from which point onward the sample is downwardly polarized.

For anisotropy values only slightly greater than the RPT value $\kappa = -\kappa_0$, a modulation of the magnetization will appear in low fields. The magnetization curve will still be reversible, but no longer exactly linear. Once the magnetic field crosses the curve $h = -\kappa\sqrt{1 + \kappa/\kappa_0}$ from above, a small modulation out of the canted phase develops continuously. That modulation fades again at the

lower curve $h = \kappa\sqrt{1 + \kappa/\kappa_0}$, and the system proceeds as before from the canted to the uniform down phase.

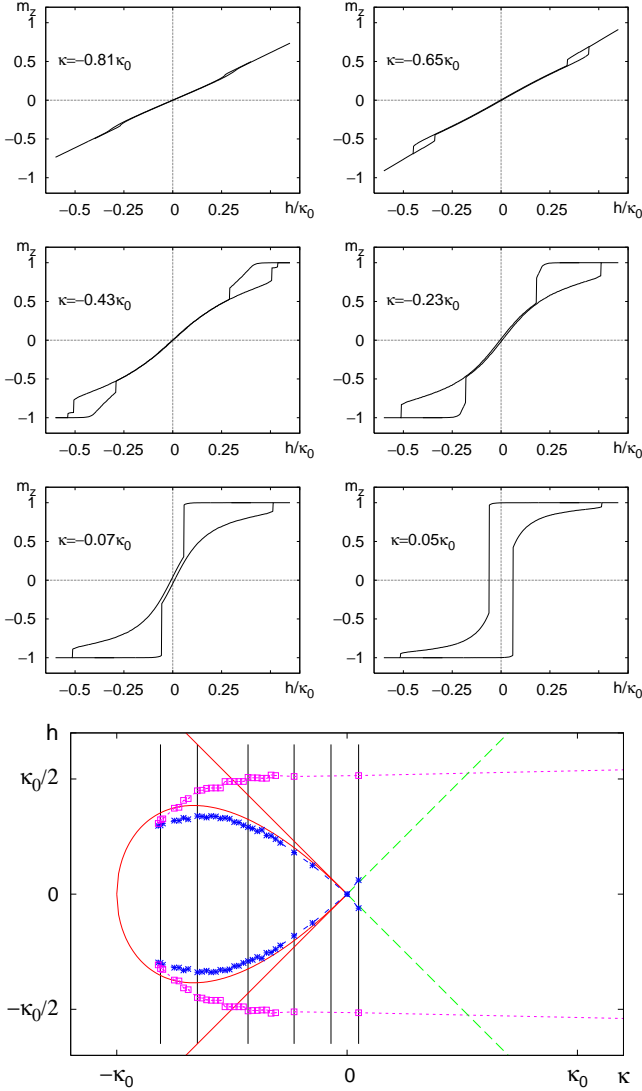


FIG. 3: (Color online) Numerical simulation of the out-of-plane hysteresis curves for several values of κ/κ_0 . The locations of these sweeps in the phase diagram are shown by vertical lines in the bottom panel.

For anisotropy values greater than κ_c , the system shows history dependence in the magnetization curve. At a slightly smaller value of h than $h = -\kappa\sqrt{1 + \kappa/\kappa_0}$, while the amplitude of the spin density wave is still on the order of 10^{-3} , the system undergoes a first-order transition from a state with small modulation and large average magnetization to one with small average magnetization and a large amplitude modulation. This stripe phase remains as the field decreases until finally the system undergoes a first-order transition in which the periodic modulation disappears. The boundary of stability of the striped phase crosses $h = \kappa$, the line beyond which the downwardly magnetized state is stable, so that for more

negative values of κ , the striped phase decays to a canted phase, while for more positive κ values, the system enters the downwardly polarized state. For example, in Fig. 3, the $\kappa = -0.81\kappa_0$ and $\kappa = -0.65\kappa_0$ magnetization curves show the striped phase decaying into the canted phase, while the other loops show a decay directly into the fully polarized phase.

For a small $\kappa > 0$, as we conduct a downward sweep of the field beginning at large positive values, the system undergoes a first-order phase transition out of the upwardly polarized state at $h = -\kappa$. There is no canted or spin-wave phase after the transition, but the simulations indicate that there is an intervening stable state with non-constant magnetization before the system decays into the downwardly polarized state. The limitations of the simulation become evident here. The periodic boundary conditions imposed in the simulation do not allow us to distinguish between a periodic state with a long period and a state with an isolated region of unfavored magnetization (soliton). Only a small number of solitons appeared within the period forced by the simulation. The considerations of Sections III B 1 and III B 2 indicate that for large enough κ the isolated soliton state is stable while the striped state is not. Whether this holds at small $\kappa > 0$ has not been determined.

The non-uniform state resulting from the first-order phase transition out of the upwardly polarized state persists until it vanishes in a first-order transition to the downward state (at $h \approx -0.5\kappa_0$ in the simulation). If one were to reverse course and increase the field again before reaching this second transition, the upward regions that had been unfavored would grow slowly rather than the system returning immediately to the totally upwardly polarized phase. This behavior accounts for the “fading contrast” seen in experiments with Co/Pt multilayers.⁸

If $\kappa > 0$ is large enough, we expect that the transition will proceed directly from an upwardly polarized state to a downwardly polarized state at $h = -\kappa$. For very large κ , neither a striped nor an isolated-soliton phase can form from the decay of the upwardly polarized state, as neither will be stable in the high fields required for the uniform state to become unstable. (See Sections III B 1 and III B 2).

There is a caveat on this expectation, however. If topologically non-trivial domains of reversed magnetization form during the transition out of the upwardly polarized phase, it may be that they are stable even in these large fields. A topologically non-trivial domain in our case is one for which the magnetization angle θ at the left end of the domain differs by a non-zero multiple of 2π from the magnetization angle at the right end. It is not unreasonable to expect the formation of such domains: if two downward regions form during the transition by rotating in opposite directions away from $\theta = 0$ then the upwardly polarized region between them will be topologically non-trivial. Since these downward regions may be initially well separated, their rotation directions are essentially independent, and so a non-trivial

upward domain will form between them roughly half the time. These non-trivial domains are the one-dimensional analog of skyrmion-type domains in two dimensions.¹⁵ Skyrmions may be the cause of the asymmetric domain nucleation observed in Co/Pt multilayers.¹⁶

The magnetization curve would look nearly the same in the case that topologically non-trivial solitons form as it would if they do not. The topologically non-trivial solitons would have small width when the field is large and so change the magnetization by a negligible amount. However, when the field is reversed after the transition, these soliton domains would grow. This would cause the system to proceed through the striped phase rather than staying downwardly polarized until $h = \kappa$. Hysteresis, then, would not be observed unless the applied field is strong enough to force the width of topological solitons down to the lattice scale, allowing them to decay.

B. $\kappa \gg \kappa_0$, the wide-stripe approximation

When the out-of-plane anisotropy is strong, the magnetization pattern is expected to consist of long up- or downwardly pointing regions, separated by short regions in which the magnetization changes rapidly from one domain type to the other. We refer to such a configuration as a “wide-stripe” phase. (Note, however, that this “phase” is continuously connected to the modulated phase at negative κ , and so not a truly distinct phase.)

It is well known that an energy advantage can be gained over a purely uniform phase through such modulation. In fact, when the out-of-plane anisotropy is very strong, the zero field model differs little from the dipolar Ising model discussed by Garel and Doniach.⁹ The two significant differences lie in the energy costs of the kinks and in topological considerations. The topological consequences of the model will be discussed in Section II B 2.

The wide-stripe configuration can be thought of as a periodic array of Bloch domain walls. These walls can be treated as elementary objects with some internal energy cost and long range interactions with other walls through the stray dipolar field. The interaction energy of two walls is logarithmic in their separation. If we define the orientation of a wall as a vector pointing from the upwardly magnetized side of the wall to the downwardly magnetized side, we find that the magnetic interaction is attractive for walls with the same orientation and repulsive for walls of opposite orientation. For a periodic structure, walls always have orientation opposite that of their nearest neighbors. It is this nearest neighbor repulsion caused by the stray magnetic field that allows for the stability of a striped phase despite the cost of the walls in exchange energy and the exchange force acting between nearby walls.

These considerations can be used to derive an analytic expression for the magnetization curve in the wide-stripe

phase:

$$\langle m_z \rangle = \frac{2}{\pi} \arcsin \left(\frac{\tilde{h}\pi^2}{4\sqrt{\tilde{\kappa}}} \exp \left(\frac{\pi}{2} \sqrt{\tilde{\kappa}} \right) \right), \quad (15)$$

where we have used the rescaled variables

$$\tilde{\kappa} = \frac{\kappa}{\kappa_0}, \quad \tilde{h} = \frac{h}{\kappa_0}. \quad (16)$$

Note that this magnetization curve is consistent with the scaling property described in Section II B. Details of the derivation, including an analytic expression for the stripe period, can be found in Appendix A.

1. Zero-soliton-density transition

As the external magnetic field is varied, the wide-stripe phase becomes dominated by the regions of magnetization favored by the magnetic field. For a strong enough magnetic field the striped phase has only narrow, widely separated regions of the unfavored magnetization (solitons). As Eq. (A15) shows, the period of the wide-stripe phase tends to infinity along the curve $\tilde{h} = -(4/\pi^2)\sqrt{\tilde{\kappa}} \exp(-\pi\sqrt{\tilde{\kappa}}/2)$. That is, the density of the unfavored solitons reaches zero. For fields above this curve, there is no stable structure with evenly spaced domains of unfavored magnetization. Note that the field at which the solitons are expelled from the system decreases exponentially with κ . For large κ the region in which stripes exist is extremely narrow. As the field varies from down to up across this region, a system that is nearly all down with a few isolated upward solitons will move quickly through the striped phase to a state that is nearly all up with a few isolated downward solitons.

2. The collapse of isolated solitons

In a perfectly isotropic sample, the field drives all the regions of unfavored magnetization to the edge of the system during the zero-soliton-density transition described above. A real sample, however, may have pinning centers where regions of opposing magnetization would be localized. These isolated solitons will persist into a much higher field, and their collapse is dependent on their topological character.

The edges of such regions interact with each other through two distinct forces. There is a long-range repulsion between them due to the dipolar stray field and a short-range exchange interaction that may be attractive or repulsive depending on the topology of the region. In addition, there is a force from the applied magnetic field that acts to increase or decrease the width of the soliton based on its polarization. If the exchange force is attractive, the boundary of stability of the isolated soliton phase is found at the field that will squeeze the soliton boundaries enough that the exchange force takes over and

the solitons collapse. If the exchange force is repulsive, the soliton must be forced to a width smaller than the lattice spacing in order to collapse, so that a phase difference of 2π between neighboring sites may be ignored as physically meaningless.

The exchange force between two domain walls a distance w apart is

$$\tilde{F}_{\text{ex}}(\tilde{w}) \sim \pm 8\tilde{\kappa} \exp\left(-\sqrt{\tilde{\kappa}}\tilde{w}\right) \text{ as } \sqrt{\tilde{\kappa}}\tilde{w} \rightarrow \infty, \quad (17)$$

where $\tilde{w} = \sqrt{\kappa_0}w/\lambda$ (see Appendix B). The force is attractive if the kinks form a non-topological soliton and repulsive if the soliton is topological.

To determine the field necessary to collapse a non-topological soliton, we take the Zeeman energy of the soliton and the energy of the stray field to be

$$\tilde{E}(\tilde{w}) = \text{const} + 2\tilde{h}\tilde{w} - \frac{8}{\pi} \ln \tilde{w} \quad (18)$$

for a single downward soliton of width w [see Eq. (A20)]. We use here the $\sqrt{\tilde{\kappa}}\tilde{w} \gg 1$ approximation, as we expect the collapse width of a non-topological soliton to be large compared to the size of the walls that border the soliton.

As the field \tilde{h} increases, the soliton is squeezed:

$$2\tilde{h} = \frac{8}{\pi\tilde{w}} - 8\tilde{\kappa} \exp\left(-\sqrt{\tilde{\kappa}}\tilde{w}\right). \quad (19)$$

Note that as \tilde{w} shrinks, the restoring force on the RHS of Eq. (19) increases at first and then reaches a maximum at

$$\tilde{w} \sim \frac{\ln \tilde{\kappa}}{2\sqrt{\tilde{\kappa}}} \quad \text{as } \tilde{\kappa} \rightarrow \infty. \quad (20)$$

A further increase in the field leads to a collapse of the soliton, as the restoring force can no longer balance the force due to the field. This justifies the approximation of large width, since for the collapse width $\sqrt{\tilde{\kappa}}\tilde{w} \sim (1/2) \ln \tilde{\kappa} \gg 1$. Hence, in a field

$$\tilde{h} \sim \frac{8\sqrt{\tilde{\kappa}}}{\pi \ln \tilde{\kappa}} \quad \text{as } \tilde{\kappa} \rightarrow \infty, \quad (21)$$

the (non-topological) soliton will collapse.

If, however, the soliton consists of a full 2π rotation of the magnetization, the restoring force never reaches a maximum. While the dipolar contribution to the force effectively disappears as the soliton width decreases to the order of the domain wall width, the repulsive exchange force increases without bound. The soliton can then only collapse when its width

$$w = \frac{\tilde{w}\lambda}{\sqrt{\kappa_0}} = \frac{2\lambda}{\sqrt{\kappa + |h|}} \operatorname{arcsinh}\left(\sqrt{1 + \frac{\kappa}{|h|}}\right), \quad (22)$$

derived in Appendix B, reaches the lattice scale.

IV. STRIPES NEAR AN EDGE

In this section, we consider the orientation of stripes near a system edge. Although we begin with a variational solution with a sinusoidal modulation, the final result is applicable to a general profile for the magnetization. We find that stripes oriented with their domain walls perpendicular to the edge are energetically favored over all other orientations except possibly that with stripes *exactly* parallel to the edge. For simplicity, we consider only the case of no applied field. The results are entirely similar when a field is applied. In particular, there is no change to Eq. (25), below. We compare these results with recent experiments on thermally evaporated Ni films.

We use the trial solution

$$m_z = a \sin(\mathbf{q} \cdot \mathbf{x} - \beta). \quad (23)$$

Here a is the amplitude of oscillations; the stripe wavevector $\mathbf{q} = (q \cos \alpha, q \sin \alpha)$ has a fixed length q ; the angle in the plane α ranges from 0 for stripes normal to the edge to $\pi/2$ for stripes parallel to the edge; the phase β will be important only for stripes parallel to the edge. In order to represent an edge at $y = 0$, we include a step function $\Theta(y)$ in all y integrals.

The energy associated with the presence of an edge comes from two sources. First, stripes at the edge generate a stray magnetic field. Second, depending on the sign of the effective anisotropy κ , the system can lower the energy by having an extra node or antinode near the edge. (The latter works only for stripes parallel to the edge.)

The long-range nature of the dipolar forces requires a certain amount of care in evaluating the edge energy. The value of the dipolar energy is sensitive to three length scales: the film thickness t , the width L_y , and the stripe period $2\pi/q$. On a computational level, keeping t and L_y finite is required to avoid ultraviolet and infrared divergences. Fortunately, the *difference* in the energies between stripes with different orientations (parameterized by the angle α) is insensitive to these length scales, as long as $\alpha \neq \pi/2$. This simplifies the computation greatly. Details of the calculation can be found in Appendix C.

For $\alpha \neq \pi/2$, the energy difference

$$\Delta E = E(\alpha, q) - E(0, q) \quad (24)$$

has no ultraviolet or infrared divergences, and is in fact independent of q (Fig. 4):

$$\frac{\Delta E(\alpha)}{\mu_0 M^2 t^2 L_x} = \frac{a^2}{8\pi} [\sin \alpha \ln(1 + \sin \alpha) + (1 - \sin \alpha) \ln \cos \alpha]. \quad (25)$$

If $\alpha = \pi/2$, the stripes are oriented exactly parallel to the edge. In that case there is a cutoff dependent term in the stray field energy difference proportional to

$$-\frac{a^2}{8\pi} \ln(qt) \cos 2\beta. \quad (26)$$

As long as the wavelength of the mode under consideration is larger than the thickness, the logarithm is negative. This term is therefore minimized when $\beta = \pi/2$ and so acts to attract the crests of the spin wave to the system edge.

There is also an additional term associated with the local part of the free energy that appears only when $\alpha = \pi/2$. It is proportional to

$$-\frac{a^2}{8}(\lambda^2 q^2 + \kappa) \frac{\sin(2\beta)}{qt}. \quad (27)$$

If the coefficient in brackets is positive (negative), this term acts to minimize the number of nodes (crests) of the spin wave that are present in the system, since each node (crest) has a cost in the exchange and anisotropy energy. The competition between the terms (26) and (27) will determine the phase of a spin-density wave parallel to the edge.

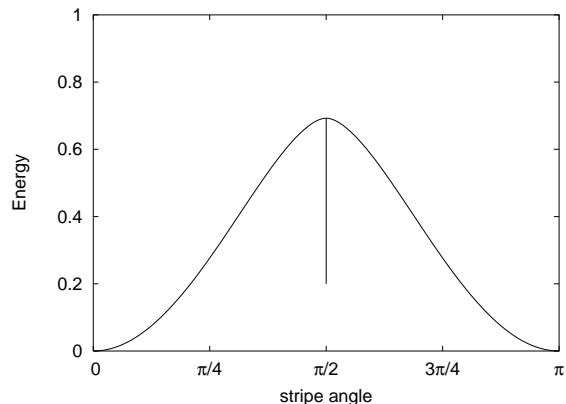


FIG. 4: Energy as a function of the angle the stripe wavevector makes with the system edge. Energy here is measured in units of $(a^2/8\pi)\mu_0 M^2 t^2 L_x$.

The addition of the phase-dependent terms above may mean that stripes parallel to the edge end up being the global minimum of energy. However, this minimum takes the form of a downward spike in the energy that occurs at an angle that would otherwise be a maximum of the energy (see Fig. 4). Even if the state with stripes parallel to the edge is the global minimum of energy, a low temperature system that begins with stripes at a random orientation is more likely to evolve toward the (metastable) minimum at $\alpha = 0$.

Since the angular dependence of the energy for $\alpha \neq \pi/2$ is independent of the wavenumber q , this result holds for any stripe profile that may be made up of higher harmonics. In that case, $a^2/2$ should be interpreted as the average value $\langle \cos^2 \theta \rangle$ of the striped state. The result is also independent of any of the material parameters because it is the energy of the stray field that causes the effect.

This result is consistent with observations made in thermally evaporated thin nickel films¹⁷ and numerical

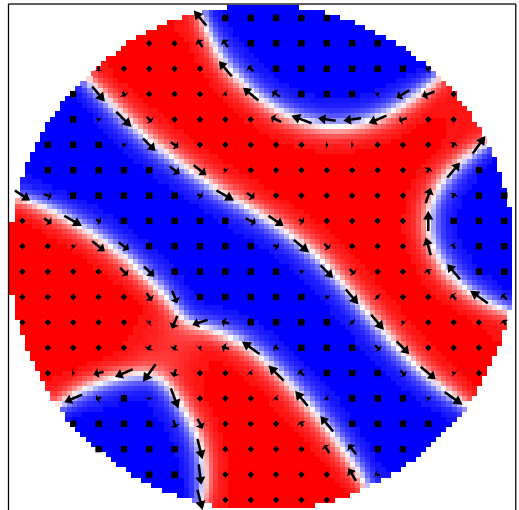


FIG. 5: (Color online) A stationary configuration obtained from a random initial state in a disk of thickness 14 nm and diameter 400 nm. Magnetization length $M = 1.4 \times 10^6$ A/m, exchange constant $A = 3.3 \times 10^{-11}$ J/m, exchange length $\lambda = 5.2$ nm, easy-axis anisotropy $K = 1.5 \times 10^6$ J/m³ yield $\kappa = 0.22$ and $\kappa_0 = 0.45$. Magnetization points up in the red (light gray) regions and down in the blue (dark gray) regions. Numerical simulation using OOMMF.¹⁸

simulations (Fig. 5) that indicate that walls meet the edges of the film at a 90° angle.

V. DISCUSSION

We have examined the properties of thin ferromagnetic films with a strong easy-axis anisotropy $K \approx K_0 = \mu_0 M^2/2$ favoring the out-of-plane component of the magnetization, with Co/Pt films as a prototype. We have found a scaling property that applies in the limit where the film thickness is the shortest length scale in the problem. In such a case the phase diagram in the field-anisotropy plane is universal if the applied field \mathbf{H} and effective anisotropy $K - K_0$ are properly rescaled. The proper variables are $\tilde{\mathbf{h}} = \mathbf{H}/(\kappa_0 M)$ and $\tilde{\kappa} = (K - K_0)/(\kappa_0 K_0)$. The parameter $\kappa_0 = (t/4\lambda)^2$ is determined by the film thickness t and the exchange length $\lambda = \sqrt{2A/\mu_0 M^2}$.

The universal phase diagram in the case of an applied field normal to the plane was determined through a combination of analytical and numerical methods focussed on uniform states and on states with a one-dimensional modulation of the magnetization, such as magnetic stripes observed near the reorientation phase transition ($K \approx K_0$). In addition to fully magnetized and canted uniform states, at least two non-uniform magnetic states were found: a spin-density wave and a striped phase. These two states are found to coexist in parts of

the phase diagram (like a gas and a liquid). The co-existence of various phases (e.g., stripes and SDW or stripes and canted) explains the rich hysteretic behavior of magnetization observed in these films. We have determined the boundaries of stability and metastability of these phases and obtained out-of-plane magnetization curves $M_{\perp}(H_{\perp})$, which have universal shapes determined by the rescaled anisotropy $\tilde{\kappa}$.

In addition to developing the zero-temperature phase diagram near the reorientation phase transition, we have expanded on previous work in the case of large out-of-plane anisotropy by finding analytic expressions for the stripe period and magnetization as functions of the applied field. We have shown that the range of field values for which a structure of evenly spaced stripes is stable is exponentially small for large anisotropy. The period of such a structure tends to infinity at a small value of the applied field. Stripes are unlikely to be found, then, at large anisotropies.

We have investigated the behavior of stripes near the film edge and found that the energy of the dipolar stray field is minimized when the stripes are perpendicular to the edge, as recently observed in Ni films. At the same time we find that a state with stripes parallel to the edge provides an opportunity to lower other terms in the free energy, e.g. the magnetic anisotropy, by registering the nodes or antinodes of magnetization at the system edge.

The behavior of the striped phase in an out-of-plane magnetic field depends on the topology of the stripes, i.e. on the direction of rotation of the magnetization. If in the absence of an applied field the colatitude angle θ oscillates between (nearly) 0 and π , the topology is trivial. As the strength of the applied field increases, the stripes of the “wrong” orientation first shrink and then disappear leaving behind a uniform state. However, if the domain walls delineating a “wrong” domain wind in the same direction (say from 0 to π and from π to 2π), this domain has a nontrivial topology. As its wall are pushed together, they feel strong repulsion mediated by exchange. As a result, such a domain will not decay until its size reaches a microscopic scale (presumably on the order of a lattice constant), at which point the phase increase from 0 to 2π can be repaired through a phase slip. These nontrivial domains are the one-dimensional analog of the skyrmion,¹⁵ a texture with a nonzero $O(3)$ winding number. Skyrmions may play a role in the magnetization reversal of thin films with high anisotropy.¹⁶

VI. ACKNOWLEDGEMENTS

We thank C.-L. Chien, S. H. Lee, N. Markovic, V. I. Nikitenko, and F. Q. Zhu for stimulating this work and for sharing unpublished data. This work was supported in part by NSF Grant DMR-0520491 and by the JHU Theoretical Interdisciplinary Physics and Astronomy Center.

APPENDIX A: PERIODIC STRUCTURE OF WIDE STRIPES

When walls between uniform regions are well separated we can treat them as nearly free defects interacting with one another mostly via their stray magnetic fields. The stray fields of other walls are thus substantially weak and can be neglected when determining the structure of a well-isolated wall. Furthermore, its own stray field can be neglected as well: the energy associated with the stray field is $\mathcal{O}(t^2)$, whereas all the other energies are $\mathcal{O}(t)$. Finally, when the anisotropy highly favors out-of-plane magnetization, the characteristic width of the domain walls is small compared to that of the stripes, so that the energy to be gained by deforming the domain walls in the presence of an external magnetic field is far outstripped by the energy to be gained by moving them. Hence the external field may be neglected as well when determining the domain wall structure.

It is convenient to use dimensionless variables for the effective anisotropy, field, coordinate, and wavenumber:

$$\tilde{\kappa} = \frac{\kappa}{\kappa_0}, \quad \tilde{h} = \frac{h}{\kappa_0}, \quad \tilde{x} = \frac{x\sqrt{\kappa_0}}{\lambda}, \quad \tilde{k} = \frac{k\lambda}{\sqrt{\kappa_0}}. \quad (\text{A1})$$

In terms of these variables, the energy (8)-(9) can be expressed as

$$\frac{E_{\text{local}}}{\mu_0 M^2 L_y t^2} = \frac{1}{4} \int d\tilde{x} \left[\frac{1}{2} \left(\frac{d\theta}{d\tilde{x}} \right)^2 - \frac{\tilde{\kappa}}{2} \cos^2 \theta - \tilde{h} \cos \theta \right] \quad (\text{A2})$$

and

$$\frac{E_{\text{stray}}}{\mu_0 M^2 L_y t^2} = -\frac{1}{4} \int \frac{d\tilde{k}}{2\pi} |\tilde{k}| |\tilde{m}_z(\tilde{k})|^2, \quad (\text{A3})$$

where we use the Fourier transform of the out-of-plane magnetization

$$\tilde{m}_z(\tilde{k}) = \int d\tilde{x} e^{i\tilde{k}\tilde{x}} \cos \theta(\tilde{x}) \quad (\text{A4})$$

We neglect for the moment the effects of the external and stray magnetic field in order to find the internal structure of a domain wall. A domain wall that interpolates between $\cos \theta = -1$ and $\cos \theta = 1$ and minimizes the sum of exchange and effective anisotropy terms in the energy above obeys:

$$\theta'^2 = \tilde{\kappa} \sin^2 \theta. \quad (\text{A5})$$

The derivative here is with respect to \tilde{x} . This is solved by $m_z = \cos \theta = \pm \tanh(\sqrt{\tilde{\kappa}}\tilde{x})$. The internal energy of each such wall is $\mu_0 M^2 t^2 L_y \sqrt{\tilde{\kappa}}/2$, not counting the interaction energy due to the stray field.

When calculating the stray field energy, it is easier to work with the \tilde{x} -derivative of the magnetization, and use the form:

$$\frac{E_{\text{stray}}}{\mu_0 M^2 L_y t^2} = -\frac{1}{4} \int \frac{d\tilde{k}}{2\pi} \frac{|\tilde{m}'_z(\tilde{k})|^2}{|\tilde{k}|}. \quad (\text{A6})$$

If the walls have small spatial extent relative to the distance between them, a periodic structure can be approximated as a sum of alternating upward and downward kinks. As such, we describe a periodic structure with period $l = \tilde{l}\lambda/\sqrt{\kappa_0}$ and upward length $w = \tilde{w}\lambda/\sqrt{\kappa_0}$ in each period by the variational solution

$$m'_z(\tilde{x}) = \int du \Delta(\tilde{w}, \tilde{l}, \tilde{x} - u) \frac{d}{du} (\tanh(\sqrt{\kappa}u)), \quad (\text{A7})$$

where

$$\Delta(\tilde{w}, \tilde{l}, u) = \sum_{n=-\infty}^{\infty} \delta(u - n\tilde{l}) - \delta(u - n\tilde{l} - \tilde{w}). \quad (\text{A8})$$

By substituting (A7) into (A6), we arrive at

$$\begin{aligned} \frac{E_{\text{stray}}}{\mu_0 M^2 V \kappa_0} &= -\frac{16\pi^3}{\tilde{\kappa} \tilde{l}^3} \sum_{j=0}^{\infty} j \frac{\sin^2(\pi j \tilde{w}/\tilde{l})}{\sinh^2(\pi^2 j/\sqrt{\tilde{\kappa}} \tilde{l})} \\ &= \frac{4(2\pi/\tilde{l})^3}{\tilde{\kappa}} \frac{d}{d\rho} \sum_{j=0}^{\infty} \sum_{n=1}^{\infty} \sin^2(\pi j \tilde{w}/\tilde{l}) e^{-2\rho j n}, \end{aligned} \quad (\text{A9})$$

where $\rho = \pi^2/\sqrt{\tilde{\kappa}}\tilde{l}$ and $V = tL_x L_y$ is the volume of the film.

Summing over j leads to an expression that can be approximated by an integral over n if $\rho \ll 1$. We thus obtain

$$\frac{E_{\text{stray}}}{\mu_0 M^2 V \kappa_0} = -\frac{4}{\pi \tilde{l}} \left[\ln(1+f) + \frac{2f}{1+f} \right], \quad (\text{A10})$$

where

$$f(\tilde{w}, \tilde{l}) = \frac{\tilde{l}^2 \tilde{\kappa}}{\pi^4} \sin^2 \left(\frac{\pi \tilde{w}}{\tilde{l}} \right). \quad (\text{A11})$$

The total internal energy of the kinks in this structure (including exchange and anisotropy) is

$$\frac{E_{\text{kinks}}}{\mu_0 M^2 V \kappa_0} = \frac{4\sqrt{\tilde{\kappa}}}{\tilde{l}}, \quad (\text{A12})$$

since there are two kinks in each period. The final contribution to the energy is the interaction with the applied magnetic field, described by the energy density

$$\frac{E_{\text{ext. field}}}{\mu_0 M^2 V \kappa_0} = -\frac{2\tilde{h}\tilde{w}}{\tilde{l}}. \quad (\text{A13})$$

Minimizing the sum of these three terms with respect to \tilde{l} and \tilde{w} leads to the following expressions for the equilibrium period and upward width of the stripes [for $\tilde{l}\sqrt{\tilde{\kappa}} \sin(\pi \tilde{w}/\tilde{l}) \gg 1$]:

$$\cos \left(\frac{\pi \tilde{w}}{\tilde{l}} \right) = -\frac{\tilde{h}\pi^2}{4\sqrt{\tilde{\kappa}}} \exp \left(\frac{\pi}{2} \sqrt{\tilde{\kappa}} \right) \quad (\text{A14})$$

and

$$\tilde{l}\sqrt{\tilde{\kappa}} \sin(\pi \tilde{w}/\tilde{l}) = \pi^2 \exp \left(\frac{\pi}{2} \sqrt{\tilde{\kappa}} \right). \quad (\text{A15})$$

Note that Eq. (A15) justifies the approximation that $\tilde{l}\sqrt{\tilde{\kappa}} \sin(\pi \tilde{w}/\tilde{l}) \gg 1$, since $\sqrt{\tilde{\kappa}}$ is large in this region of the phase diagram.

These equations can be solved to give:

$$\tilde{w} = \frac{2 \arccos(-\tilde{h}/\tilde{h}_0)}{\pi \sqrt{\tilde{h}_0^2 - \tilde{h}^2}} \quad (\text{A16})$$

and

$$\tilde{l} = \frac{2}{\sqrt{\tilde{h}_0^2 - \tilde{h}^2}} \quad (\text{A17})$$

with $\tilde{h}_0 = -(4/\pi^2)\sqrt{\tilde{\kappa}} \exp(-\pi\sqrt{\tilde{\kappa}}/2)$.

For $\tilde{h} = 0$ the above equations reduce to $\tilde{w} = \tilde{l}/2$ (i.e., no net magnetization), and a stable period of

$$l = \frac{\lambda \tilde{l}}{\sqrt{\kappa_0}} = \frac{\pi^2 \lambda}{\sqrt{\kappa}} \exp \left(\frac{\pi}{2} \sqrt{\frac{\kappa}{\kappa_0}} \right). \quad (\text{A18})$$

Since the average magnetization $\langle m_z \rangle = 2\tilde{w}/\tilde{l} - 1$, Eq. (A14) can be rewritten to give the magnetization curve for large κ :

$$\langle m_z \rangle = \frac{2}{\pi} \arcsin \left(\frac{\tilde{h}\pi^2}{4\sqrt{\tilde{\kappa}}} \exp \left(\frac{\pi}{2} \sqrt{\tilde{\kappa}} \right) \right). \quad (\text{A19})$$

Further, note that as $\tilde{h} \rightarrow -\tilde{h}_0$, the period \tilde{l} tends to infinity while the upward width stays finite [$\tilde{w} \rightarrow (\pi/4\sqrt{\tilde{\kappa}}) \exp(\pi\sqrt{\tilde{\kappa}}/2)$]. For larger fields there is no stable periodic structure of this type.

If, instead of a periodic structure, we are interested in the energy of a single soliton, we take $l \rightarrow L_x \gg w$ in Eqs. (A10)-(A13), so that $f(\tilde{w}, \tilde{l}) \approx \tilde{\kappa}\tilde{w}^2/\pi^2$ leading to

$$\begin{aligned} \frac{4E}{t^2 L_y \mu_0 M^2} &\approx 4\sqrt{\tilde{\kappa}} - 2\tilde{h}\tilde{w} - \frac{4}{\pi} \left[\ln \left(1 + \frac{\tilde{\kappa}\tilde{w}^2}{\pi^2} \right) + \frac{2\tilde{\kappa}\tilde{w}^2}{\pi^2 + \tilde{\kappa}\tilde{w}^2} \right] \\ &\approx \text{const} - 2\tilde{h}\tilde{w} - \frac{8}{\pi} \ln \tilde{w} \end{aligned} \quad (\text{A20})$$

for an upward soliton of width w when $\tilde{\kappa}\tilde{w}^2 \gg 1$.

APPENDIX B: SOLITONS AND THE EXCHANGE FORCE BETWEEN DOMAIN WALLS

The energy of a single soliton given above by Eq. (A20) does not take into account the exchange interaction between the domain walls bounding the soliton. This interaction will become important as the walls move closer together.

If we wish to find the effective force due to the exchange interaction, we must first find stable soliton solutions to the Lagrange equation associated with the energy (A2). We will ignore the effects of the stray magnetic field (in the limit of large κ with $t \ll \lambda/\sqrt{\kappa - |h|}$). Since the force on the walls due to the magnetic field is known, the stable width of a soliton can be used to find the effective exchange force between the walls that must be acting to oppose the field.

We will apply the boundary conditions $\theta(\pm\infty) = \pi$ and $\theta'(\pm\infty) = 0$, thus describing an upward soliton in a downwardly polarized background. We obtain from (A2) that

$$\frac{\theta'^2}{2} = \frac{1}{2}\tilde{\kappa}\sin^2\theta - \tilde{h}(1 + \cos\theta), \quad (\text{B1})$$

where $\tilde{\kappa} = \kappa/\kappa_0$, $\tilde{h} = h/\kappa_0$, and $\tilde{x} = x\sqrt{\kappa_0}/\lambda$, as in Eqs. (A2)-(A3).

We expect different solutions to this equation for $\tilde{h} > 0$ and $\tilde{h} < 0$. If $\tilde{h} > 0$, then the soliton is favored by the field, and the background is unfavored, held in place only by the out-of-plane anisotropy. In order to balance the force of the field, the exchange interaction in this case will attract the walls of the soliton to one another.

The corresponding solution to Eq. (B1) at $\tilde{h} > 0$ is

$$\cos\theta = -1 + \frac{2(1 - \tilde{h}/\tilde{\kappa})}{1 + (\tilde{h}/\tilde{\kappa})\sinh^2(k\tilde{x})}, \quad (\text{B2})$$

where $k = \sqrt{\tilde{\kappa} - \tilde{h}}$.

Note that $\cos\theta(0) = 1 - 2\tilde{h}/\tilde{\kappa}$ is the maximum value of $\cos\theta$ in this solution. Nowhere is there full upward polarization, so this solution describes a non-topological soliton, in which there is no net rotation of the magnetization between the ends of the system.

If, on the other hand, $\tilde{h} < 0$, then the background is favored by the field and the soliton is not. The exchange force between the walls of the soliton must be repulsive in order to balance the force of the field squeezing the walls together. This is accomplished by a topological soliton solution, in which the magnetization rotates by a full 2π between the ends of the system. The solution to Eq. (B1) in this case ($\tilde{h} < 0$) is

$$\cos\theta = -1 + \frac{2(1 - \tilde{h}/\tilde{\kappa})}{1 - (\tilde{h}/\tilde{\kappa})\cosh^2(k\tilde{x})}. \quad (\text{B3})$$

Again, $k = \sqrt{\tilde{\kappa} - \tilde{h}}$.

Note that in this case, $\cos\theta(0) = 1$ for any value of \tilde{h} . The 2π rotation of the magnetization forces the magnetization to point upward in the center of the soliton in any field. This is the reason for the repulsive exchange force. If the soliton is squeezed, the magnetization is forced to move from down to up and back in a shorter distance.

If we set $\cos\theta = 0$ in Eq. (B2) to find the locations $\pm\tilde{x}_0$ of the kinks bounding the non-topological soliton,

we obtain

$$\tilde{h} = \frac{\tilde{\kappa}}{1 + \cosh^2(\tilde{x}_0\sqrt{\tilde{\kappa} - \tilde{h}})} \approx 4\tilde{\kappa}\exp(-2\sqrt{\tilde{\kappa}}\tilde{x}_0) \quad (\text{B4})$$

for large $\tilde{\kappa}$. Since the force of the field is $2\tilde{h}$ acting to separate the kinks, the (rescaled) exchange force in the non-topological case is

$$\tilde{F}_{\text{ex}} = -8\tilde{\kappa}\exp(-\sqrt{\tilde{\kappa}}\tilde{w}). \quad (\text{B5})$$

Note that $\tilde{w} = 2\tilde{x}_0$, since the kinks are at $\tilde{x} = \pm\tilde{x}_0$.

Similarly, if we set $\cos\theta = 0$ in Eq. (B3), we obtain

$$-\tilde{h} = \frac{\tilde{\kappa}}{-1 + \sinh^2(\tilde{x}_0\sqrt{\tilde{\kappa} - \tilde{h}})} \approx 4\tilde{\kappa}\exp(-2\sqrt{\tilde{\kappa}}\tilde{x}_0) \quad (\text{B6})$$

for large $\tilde{\kappa}$ and moderate width. Since the force of the field is now acting to compress the kinks, the (rescaled) exchange force in the case in which the soliton is topological is $\tilde{F}_{\text{ex}} = +8\tilde{\kappa}\exp(-\sqrt{\tilde{\kappa}}\tilde{w})$, a repulsive force.

If the field is very high, the kinks in the topological case will be forced close together, so that the large $\sqrt{\tilde{\kappa}}\tilde{w}$ approximation is no longer valid. The soliton will not collapse, however, until the width [obtained by solving Eq. (B6) for $\tilde{w} = 2\tilde{x}_0$]

$$w = \frac{\tilde{w}\lambda}{\sqrt{\kappa_0}} = \frac{2\lambda}{\sqrt{\kappa + |h|}} \operatorname{arcsinh}\left(\sqrt{1 + \frac{\kappa}{|h|}}\right) \quad (\text{B7})$$

is on the order of the lattice spacing.

APPENDIX C: ENERGY OF STRIPES NEAR AN EDGE

The energy of a two-dimensional thin-film system with magnetic field oriented normal to the plane of the sample and no bulk charge is

$$\begin{aligned} \frac{E}{\mu_0 M^2 t} &= \int d^2x \left[\frac{\lambda^2 |\nabla m_z|^2}{2(1 - m_z^2)} - \frac{\kappa}{2} m_z^2 - h m_z \right] \\ &\quad - \frac{t}{4} \int \frac{d^2k}{(2\pi)^2} |k| |m_z(\mathbf{k})|^2. \end{aligned} \quad (\text{C1})$$

Here $m_z(\mathbf{k})$ represents the two-dimensional Fourier transform of m_z . In order to include the effects of a system edge, we will include a step function $\Theta(y)$ as a factor in all the y -integrals that appear. For simplicity we discuss the case of zero applied field, $h = 0$, only.

We use a trial solution with a single wave number and propagation direction. We will be comparing the energy of solutions with different values of the angle between the propagation direction and the system edge. We label this angle α . Our trial solution is

$$m_z = a \sin(\mathbf{q} \cdot \mathbf{x} - \beta), \quad (\text{C2})$$

where a is the modulation amplitude, $\mathbf{q} = (q \cos \alpha, q \sin \alpha)$, and α ranges from 0 for stripes running perpendicular to the edge to $\pi/2$ for stripes running parallel to the edge. In order to evaluate the energy, we use the form

$$\Theta(y) = \int \frac{dp}{2\pi} \frac{ie^{ipy}}{p + i\epsilon} \quad (\text{C3})$$

for the step function in order to regularize the infrared divergence. Here $L_y = 1/\epsilon$ is the extent of the system in the y -direction. Where necessary, we also use the inverse of the sample thickness as an ultraviolet cutoff in momentum space integrals.

1. $\alpha \neq \pi/2$

As long as stripes are not parallel to the edge, trial solutions with different values of β are related to one another by a translation in the x direction. Since the integration in Eq. (C1) is carried out over all x , the energy is independent of the phase β . Further, the total contribution of the local terms in the energy is the same for any orientation other than $\alpha = \pi/2$. The dependence of energy on the orientation then reflects the effect of the dipolar stray field alone.

By inserting the trial solution (C2) into the stray field term in Eq. (C1) using the form (C3) for the step function, we obtain directly that the contribution of the stray field to the energy is:

$$\frac{E_{\text{stray}}(\alpha, q)}{E_0} = -\frac{a^2}{16} \int \frac{dp}{2\pi} \left(\frac{\sqrt{q^2 + 2qp \sin \alpha + p^2}}{p^2 + \epsilon^2} + \frac{\sqrt{q^2 - 2qp \sin \alpha + p^2}}{p^2 + \epsilon^2} \right), \quad (\text{C4})$$

where we introduce a characteristic energy scale

$$E_0 = \mu_0 M^2 t^2 L_x. \quad (\text{C5})$$

This integral requires both infrared and ultraviolet cut-offs. The inverse thickness $1/t$ serves to cut off the ultraviolet divergence in the integral and $\epsilon = 1/L_y$ the infrared. However, the difference $E_{\text{stray}}(\alpha, q) - E_{\text{stray}}(0, q)$ is not sensitive to these cutoffs and can be evaluated in the limits $t \rightarrow 0$ and $1/\epsilon = L_y \rightarrow \infty$. Remarkably, the difference is also independent of the wavenumber q . By subtracting $E_{\text{stray}}(0, q)/E_0$ from Eq. (C4) and performing the p integration, we obtain

$$\frac{E_{\text{stray}}(\alpha, q) - E_{\text{stray}}(0, q)}{E_0} = \frac{a^2}{8\pi} f(\alpha), \quad (\text{C6})$$

where the function

$$f(\alpha) = \sin \alpha \ln(1 + \sin \alpha) + (1 - \sin \alpha) \ln(\cos \alpha) \quad (\text{C7})$$

has a minimum at $\alpha = 0$, when the stripes are normal to the edge.

2. $\alpha = \pi/2$

When stripes are parallel to the edge, the energy also depends on the phase β . To leading order in t and ϵ ,

$$\frac{E(\pi/2, q) - E(0, q)}{E_0} = \frac{a^2}{8\pi} \left[-\frac{\pi(\kappa + \lambda^2 q^2) \sin(2\beta)}{qt} + \ln(2) - \ln(qt) \cos(2\beta) \right]. \quad (\text{C8})$$

In addition to the energy of the stray field, this expression reflects the energy of anisotropy and exchange, both of which are sensitive to the positions of nodes relative to the edge.

The overall energy dependence, including a dip at $\alpha = \pi/2$, is shown in Fig. 4. Depending on the parameters of the film, the global minimum may be either at $\alpha = 0$ or at $\alpha = \pi/2$. However, even if the global minimum is at $\pi/2$, the system may not easily find that configuration and remain in the metastable state with the stripes normal to the edge ($\alpha = 0$).

-
- ¹ J. E. Davies, O. Hellwig, E. E. Fullerton, G. Denbeaux, J. B. Kortright, and K. Liu, Phys. Rev. B **70**, 224434 (2004).
 - ² L. B. Steren, J. Milano, V. Garcia, M. Marangolo, M. Ed-drief, and V. H. Etgens, Phys. Rev. B **74**, 144402 (2006).
 - ³ O. Schulte, F. Klose, and W. Felsch, Phys. Rev. B **52**, 6480 (1995).
 - ⁴ O. Donzelli, D. Palmeri, L. Musa, F. Casoli, F. Albertini, L. Pareti, and G. Turilli, J. Appl. Phys. **93**, 9908 (2003).
 - ⁵ A. Marty, Y. Samson, B. Gilles, M. Belakhovsky, E. Dudzik, H. Durr, S. S. Dhesi, G. van der Laan, and J. B. Goedkoop, J. Appl. Phys. **87**, 5472 (2000).
 - ⁶ T. Shono, T. Hasegawa, T. Fukumura, and F. Matsukura, H. Ohno, Appl. Phys. Lett., **77**, 1363 (2000).
 - ⁷ G. Xiang, A. W. Holleitner, B. L. Sheu, F. M. Mendoza, O. Maksimov, M. B. Stone, P. Schiffer, D. D. Awschalom,

- and N. Samarth, Phys. Rev. B **71**, 241307 (2005).
- ⁸ X. M. Cheng, V. I. Nikitenko, A. J. Shapiro, R. D. Shull, and C. L. Chien, J. Appl. Phys. **99**, 08C905 (2006).
- ⁹ T. Garel and S. Doniach, Phys. Rev. B **26**, 325 (1982).
- ¹⁰ Y. Yafet and E. M. Gyorgy, Phys. Rev. B **38**, 9145 (1988).
- ¹¹ A. Berger and R. P. Erickson, J. Magn. Magn. Mater. **165**, 70 (1997).
- ¹² A. B. Kashuba and V. L. Pokrovsky, Phys. Rev. B **48**, 10335 (1993).
- ¹³ Ar. Abanov, V. Kalatsky, V. L. Pokrovsky, and W. M. Saslow, Phys. Rev. B **51**, 1023 (1995).
- ¹⁴ W. H. Press, B. P. Flannery, S. A. Teukolsky, and W. T. Vetterling, *Numerical recipes in C: the art of scientific computing* (Cambridge, New York, 1988).
- ¹⁵ A. A. Belavin and A. M. Polyakov, Pis'ma ZhETF **22**, 503 (1975) [JETP Lett. **22**, 245 (1975)].

- ¹⁶ Y. L. Iunin, Y. P. Kabanov, V. I. Nikitenko, X. M. Cheng, D. Clarke, O. A. Tretiakov, O. Tchernyshyov, A. J. Sharpiro, R. D. Shull, and C. L. Chien, Phys. Rev. Lett. (to be published).
- ¹⁷ S. H. Lee, F. Q. Zhu, N. Markovic, and C.-L. Chien (unpublished).
- ¹⁸ M. J. Donahue and D. G. Porter, OOMMF User's Guide, Version 1.0, in *Interagency Report NISTIR 6376* (NIST, Gaithersburg, 1999). <http://math.nist.gov/oommf/>